

1 **Refined burned-area mapping protocol using Sentinel-2 data**
2 **increases estimate of 2019 Indonesian burning**

3 David L.A. Gaveau¹ Adrià Descals², Mohammad A. Salim¹, Douglas Sheil³, Sean Sloan⁴

4 ¹ TheTreeMap Bagadou Bas 46600 Martel, France

5 ² CREAF, Centre de Recerca Ecològica i Aplicacions Forestals, E08193 Bellaterra (Cerdanyola de Vallès),
6 Catalonia, Spain

7 ³ Forest Ecology and Forest Management Group, Wageningen University & Research, PO Box 47, 6700 AA,
8 Wageningen, The Netherlands

9 ⁴ Department of Geography, Vancouver Island University, Nanaimo, BC, Canada &

10 Correspondence to: David Gaveau (d.gaveau@thetree.com)

11 **Abstract**

12 Many nations are challenged by landscape fires. A confident knowledge of the area and distribution of burning is
13 crucial to monitor these fires and to assess how they might best be reduced. Given the differences that arise using
14 different detection approaches, and the uncertainties surrounding burned-area estimates, their relative merits
15 require evaluation. Here we propose, illustrate, and examine one promising approach for Indonesia.

16 Drawing on Sentinel-2 satellite time-series analysis, we present and validate new 2019 burned-area estimates for
17 Indonesia. The corresponding burned-area map is available at: <https://doi.org/10.5281/zenodo.4551243> (Gaveau
18 et al., 2021). We show that >3.11 million hectares (Mha) burned in 2019. This burned-area extent is double the
19 Landsat-derived Official estimate of 1.64 Mha from the Indonesian Ministry of Environment and Forestry, and
20 50% more than the MODIS MCD64A1 burned-area estimate of 2.03 Mha. Though we observed proportionally
21 less peatland burning (31% versus 39% and 40% for the Official and MCD64A1 products, respectively), in
22 absolute terms we still observed a greater area of peatland affected (0.96 Mha) than the official estimate (0.64
23 Mha). This new burned-area dataset has greater reliability as these alternatives, attaining a user's accuracy of
24 97.9% (CI: 97.1%-98.8%) compared to 95.1% (CI: 93.5%-96.7%) and 76% (CI: 73.3%-78.7%), respectively. It
25 omits fewer burned areas, particularly smaller- (<100 ha) to intermediate-sized (100 ha -1000 ha) burns, attaining
26 a producer's accuracy of 75.6% (CI: 68.3%-83.0%) compared to 49.5% (CI: 42.5%-56.6%) and 53.1% (CI:
27 45.8%-60.5%), respectively. The frequency-area distribution of the Sentinel-2 burns follows the apparent fractal-
28 like power-law or "pareto" pattern often reported in other fire studies, suggesting good detection over several
29 magnitudes of scale. Our relatively accurate estimates have important implications for carbon-emission
30 calculations from forest and peatland fires in Indonesia.

31

32 **1. Introduction**

33 Accurate burned area maps are key to characterizing landscape fires, clarifying emissions and identifying the
34 probable causes. Such information is needed to target interventions, to assess policies and practices intended to
35 reduce or control fires, such as law enforcement and restoration of fire-prone degraded lands, and to measure
36 progress to international climate commitments (Sloan et al., 2021). Here, we focus on Indonesia where recurring
37 forest and peatland fires have become an international crisis (Tacconi, 2016). These concerns arise from the large
38 carbon emissions associated with these fires, and the impact of associated aerosol emissions for human health in
39 the wider region (Van der Werf et al., 2008; Marlier et al., 2013). Although fires have occurred locally in Southeast
40 Asia for millennia, they are increasingly frequent in Indonesia's disturbed forests and deforested peatlands (Field
41 et al., 2009; Gaveau et al., 2014). The causes and motivations of fire use can be complex (Dennis et al., 2005), but
42 many are lit to create or maintain agricultural land (Gaveau et al., 2014; Adrianto et al., 2020). Most fires occur
43 during drier months (July to October) and the threats are greatly heightened during years of anomalously low
44 rainfall (Sloan et al., 2017; Field et al., 2016). During 2015, a strong El Niño-induced drought year, fires burned
45 an estimated 2.6 million hectares according to official estimates (Sipongi, 2020). Although 2015 burning was
46 approximately half as extensive as 1997, the most severe El Niño and fire season on record (Fanin and Werf,
47 2017), about 50% more peatlands burned (Fanin and Werf, 2017). The 2015 fires emitted between 0.89 and 1.5
48 billion tons of CO₂ equivalent (Huijnen et al., 2016; Lohberger et al., 2018; Van Der Werf et al., 2017),
49 representing about half of Indonesia's greenhouse gas emissions for that year (Gütschow et al., 2019). In
50 Palangkaraya, the capital city of Central Kalimantan province, daily average particulate matter (PM₁₀)
51 concentrations often reached 1000 to 3000 µg m⁻³ amongst the worst sustained air quality ever recorded worldwide

52 (Wooster et al., 2018). Over half a million people suffered respiratory problems in the aftermath, and between
53 12,000 and 100,000 premature deaths were estimated (Kopplitz et al., 2016; Crippa et al., 2016). Other impacts
54 include loss and degradation of habitats with high conservation values, and the associated consequences for
55 impacted wildlife (Harrison et al., 2016).

56

57 In response to the catastrophic 2015 fires, the Indonesian government instituted several ambitious schemes
58 including fire bans enforced by dedicated command posts (Sloan et al., 2021) and an ambitious national program
59 of peatland restoration (Carmenta et al., 2020). Despite the investment in these approaches and measures, and
60 initial success, severe burning struck Indonesia again in late 2019. While Sloan et al. (2021) suggest that 2019 fire
61 activity was lower than expected given the severe drought conditions, the total number of MODIS active-fire
62 detections in late 2019 on peatlands was still amongst the greatest recorded since 2001 (Sloan et al., 2021).
63 However, counts of active-fire detections don't provide estimates of area burned (Tansey et al., 2008) and for
64 2019 such estimates remain uncertain.

65

66 Those wishing to assess and monitor burned areas have various approaches to consider. Several global burned
67 area products generated using coarse-resolution satellites (>250 m) can be applied over Indonesia. These include
68 the FireCCI41 product derived from Envisat-MERIS (Alonso-Canas and Chuvieco, 2015), the FireCCI51 and
69 MCD64A1 products derived from TERRA&AQUA-MODIS (Giglio et al., 2018; Lizundia-Loiola et al.,
70 2020), the FireCCILT10 product derived from AVHRR (Otón et al., 2019) and the C3SBA10 product derived
71 from Sentinel-3 (Lizundia-Loiola et al., 2021). Currently, the MCD64A1 (collection 6), based on MODIS 500 m
72 bands, is considered one of the most accurate global product (Chuvieco et al., 2019), with omission and
73 commission errors of 40% and 22% globally for the 'burned' class (Giglio et al., 2018). This validation is based
74 on independent globally distributed visually interpreted reference satellite data, however none over Indonesia.
75 These coarse-resolution datasets generally omit small-scale fires and, thus, the reported burned area is
76 underestimated (Ramo et al., 2021). This has motivated research in the use of medium-resolution satellites (10 to
77 30 meters) such Sentinel-1 (Lohberger et al., 2018 in Indonesia), Sentinel-2 (Chuvieco et al. 2018 in Sub-Saharan
78 Africa), and the Landsat constellation (Hawbaker et al., 2017 in North America) to produce more detailed burned
79 area maps. Lohberger et al. (2018) reported 4.6 Mha burned in 2015 in Indonesia, nearly double the estimate of
80 2.6 Mha from the Indonesian Ministry of Environment and Forestry (MOEF), using visual interpretations of time-
81 series Landsat-8 imagery (Sipongi, 2020).

82

83 For year 2019, The MOEF (hereafter 'Official estimate') estimated that 1.64 Mha burned in 2019 (Sipongi, 2020),
84 while the MCD64A1 (collection 6) indicated 2.03 Mha burned in 2019. The coarse 500-m spatial resolution
85 MCD64A1 data omit smaller fires and thus likely overlook many localized events. The Landsat imagery
86 underlying the Official estimates are, while finer scale, observed every 16 days at best (typically much less due to
87 cloud and smoke), meaning that many burns may remain undetected. Also, smaller-scale and/or dispersed fire
88 activity may be underestimated, considering the challenges of their visual interpretation and delineation. Visual
89 interpretation entails a manual delineation of burns perimeters, which yields accurate results for large burn
90 mapping at local scales, but is very time consuming at large spatial scales, particularly when mapping small fires.
91 A thorough accuracy assessment is also not available for the official burned-area products. Given the unknown
92 errors around burned-area estimates, and the differences between them, the accuracy, and merits of different
93 mapping approaches over Indonesia require formal examination.

94

95 Here, we present new and validated 2019 burned-area estimates for Indonesia using a time-series of the
96 atmospherically corrected surface reflectance multispectral images (level 2A product) taken by the Sentinel-2 A
97 and B satellites. With higher spatial resolution (20-m) and more frequent observations (5-day revisit time), the
98 Sentinel-2A and B satellites offer relatively comprehensive and accurate burned-area mapping (Huang et al., 2016;
99 Ramo et al., 2021). We used the Google Earth Engine (Gorelick et al., 2017), thus permitting wide application.
100 We also developed an independent reference dataset to compare the accuracy of our estimate against the Official
101 and MCD64A1 burned-area maps. Given the lack of objectively distributed ground truthing, we sought ways to
102 extract reference sites by visually detecting a smoke plume, burn, or heat source (flaming front, or hotspot) from
103 the archive of original Sentinel-2 images. Finally, we examined differences in terms of burn-size frequency
104 distributions among these three burned-area estimates to examine spatial patterns.

105

106 **2. Methods**

107 *2.1. Summary of methods*

108 A burned area is identified by alteration of vegetation cover and structure along with deposits of char and ash. We
109 mapped such areas using a change-detection approach, i.e. by comparing Sentinel-2 infrared signals recorded
110 before and after a burning event (Liu et al., 2020). We analyzed a time-series of the Normalized Burned Area
111 Ratio (see section 2.2) to assemble two national composite images depicting the spectral condition of vegetation
112 shortly before and shortly after a disturbance (Figure 1). These composites represent a convenient way to capture
113 the entire burned landscape stored in just two image files. Although we refer to these images as “pre- and post-
114 fire composites”, they also capture damage due to other causes, for example a cutting event (e.g. mechanical
115 conversion to agriculture, to timber plantation, to roads, population centers, mining or natural timber harvesting),
116 a disease, strong winds, floods, or landslides (Gaveau et al., 2021). After the production of the pre- and post-fire
117 composites, we used a “Random Forest” classification model (see section 2.3) trained on visually identified pairs
118 of pre- and post-fire pixels to confirm if the spectral changes indicating vegetation damage corresponded to a
119 burning event. Third, three independent interpreters assembled a reference dataset by visually identifying burns
120 in the original time-series Sentinel-2 images. Fourth, we assessed our burned-area map, as well as the Official and
121 MCD64A1 burned-area maps, against our reference dataset to gauge the reliability and accuracy of the three
122 burned-areas products. Finally, we tested whether, and how, the three burned-area estimates differed in their
123 tendencies to incorporate burns of different sizes.

124

125 *2.2. Pre- and post-fire Sentinel-2 national composite images of 2019*

126 Here, we describe our automated procedure to create a national pair of pre- and post-fire composites from 47,220
127 original Sentinel-2 images acquired between 01 November 2018 and 31 December 2019. Prior to creating the
128 composites, we removed non-valid pixels using the Sentinel-2 imagery quality flag (this flag provides information
129 about clouds, cloud shadows, and other non-valid observations) produced by the ATCOR algorithm and included
130 in the atmospherically-corrected surface reflectance multispectral images of the Sentinel-2 A and B satellites
131 Surface Reflectance products (Level 2A product) (Fletcher, 2012).

132 A time series of the Normalized Burned Ratio (NBR), given as $(\text{NIR}-\text{SWIR}) / (\text{NIR}+\text{SWIR})$, represents a
133 convenient index to detect the approximate day when the vegetation was damaged. Before damage, vegetated

134 pixels register high NBR values close to 1 because reflectance in near-infrared spectrum (NIR; wavelength=0.842
135 μm ; Band 8) is high due to the chlorophyll content of the vegetation (open circles before a disturbance, in this
136 case a fire, in Figure 2). The NBR of damaged vegetation typically declines abruptly towards 0 (or ≤ 0 for severe
137 damage) because the NIR reflectance declines due to chlorophyll and leaf destruction, while the reflectance of
138 short-wave-infrared spectrum (SWIR; wavelength = 1.610 μm or 2.190 μm ; Band 11 or Band 12) increases due
139 to dead or charred material and exposed ground cover. NBR values ≤ 0 are often apparent for several weeks after
140 severe burning or clear-cutting. We analyzed NBR time series for approximately 94.5 billion 400 m^2 pixels
141 (Indonesia's landmass =198 Mha). We describe the procedure to detect drops in the NBR time series in the
142 following paragraph.

143 We detected drops in NBR time series with a moving-window approach. A moving window scanned NBR values
144 three months prior and one month after the central day of the window. The output value of the moving window
145 (blue dots in Figure 2) is the difference between average NBR values observed before and after the central day.
146 The NBR average after the central day included the value at the central day. The difference between the average
147 NBR values was estimated every 2 days in the time series, skipping the day of year that was an odd number (day
148 of year equal to 2, 4, 6, 8...). Although Sentinel-2 has a temporal resolution of 5 days, the overlap between satellite
149 passes may increase the temporal resolution regionally up to 2 days at the equator. Thus, we estimated the NBR
150 difference (dNBR) every 2 days instead of 5 days. Taking this into consideration, our 'disturbance' date estimate
151 has a maximum temporal precision of 2 days in specific regions, but generally 5 days when satellite passes do not
152 overlap. The day of the year when dNBR reached a maximum corresponded to the moment NBR dropped most
153 markedly in each pixel, flagging a disturbance to the pixel's vegetation potentially caused by fire. At this
154 date, we created a pair of pre- and post-fire pixels by selecting the median Red, NIR and SWIR spectral values
155 acquired three months before and one month after the disturbance. We selected a one-month window rather than
156 a three-month window to compute the post-fire image to maximize our chances to detect recent burns, given that
157 burned areas on degraded lands and savanna tend to re-green rapidly. We repeated this procedure for
158 approximately 94.5 billion pixels to assemble two national composite images depicting the spectral condition of
159 vegetation shortly before and shortly after a disturbance (Figure 1).

160 *2.3. Supervised burned/unburned classification.*

161 We used the Random Forest supervised classification algorithm (Breiman, 2001), available via the Google Earth
162 Engine to determine whether the spectral changes detected by the pre- and post-fire composites corresponded to
163 a burning event, and subsequently classify burned areas. Supervised classifiers require 'training data', that is,
164 exemplary spectral signatures of 'burned' and 'unburned' lands in the present case, to guide the algorithm to
165 reliably classify the target classes. The spectral signatures (i.e., the reflectance values in the pre- and post-fire
166 composite images) are the predictive variables of the classification model. The features used in the Random Forest
167 are the bands of Sentinel-2 in the pre- and post-fire composites plus their respective NBR index. We excluded the
168 bands at 60-meter spatial resolution (bands B1, B9, and B10) since these bands present a low spatial resolution
169 for the aim of the study. Therefore, we used a total of 22 features; the NBR and bands B2, B3, B4, B5, B6, B7,
170 B8, B8A, B11, and B12 of the pre and post-composites.

171 We used a 10-fold cross-validation to assess the accuracy obtained with a set of different parameters in the
172 Random Forest. The splitting 'train-test' in the cross-validation was done only with the training dataset, since the
173 reference dataset used for the final validation must be completely independent of the training and model
174 parametrization. The two parameters that we tuned were the *number of trees* and the *minimum leaf size*. Random

175 Forest is an ensemble classifier composed of several Decision Trees; the parameter *number of trees* represents the
176 number of Decision Trees in the Random Forest. The *minimum leaf size* represents the minimum number of
177 samples that result from a splitting node at the Decision Tree. We found that a *minimum leaf size* equal to 1
178 performed the best on average and, thus, we used this value. We selected a conservative *number of trees*, 50, to
179 ensure the good performance of the Random Forest. We did not set any limit to the maximum nodes in each tree
180 and the variable to split in the random forest was set to the square root of the number of variables, which is the
181 common practice among machine learning practitioners and the default configuration in Google Earth Engine.

182 The required number of points used to train our supervised classification model (here a Random Forest) depends
183 on the spectral separability of the classes (in our case two classes: “burned” and “unburned”). The pixels that
184 show the burn present a singular spectral signature and, for this reason, it is necessary to collect a large amount of
185 training points. We collected training points until we were satisfied with the results of the classification by visually
186 comparing the resulting burned area map against the pre- and post-fire composites. We trained the Random Forest
187 algorithm using 988 independent training pixels (Supplementary Figure S1 for locations), being point coordinates
188 labelled as either ‘burned’ (317 points) or as ‘unburned’ (671 points). These pixels were selected by visual
189 interpretation of the pre- and post- fire image composites. Burned areas show a distinctive dark (low albedo)
190 brown/red color in the SWIR-NIR-Red composite image when displayed as Red-Green-Blue channels (Figure 1).
191 The training pixels were collected across landcover types (Supplementary Table S1 for landcover types) to ensure
192 the representativeness of the training dataset and the satisfactory generalization of the classification model across
193 Indonesia. We selected training pixels focused explicitly on medium-to-high burn severity, i.e. areas where the
194 distinctive red color in the SWIR-NIR-Red composite image looked the darkest, indicating that all or most of the
195 vegetation/soil burned. This aspect of the method minimized “false positives” but may exclude areas with implied
196 low-burn severity or low-visibility impacts, such as understorey fires (below an intact forest canopy, see e.g., van
197 Nieuwstadt and Sheil, 2005. By prioritizing confident identification of fires over absolute burned-area coverage,
198 as well as by duly validating our estimates, this approach avoids the problems caused by frequent false positives
199 (Rochmyaningsih, 2020).

200 We assessed burn severity during algorithm training based on visual interpretation. RGB composites with bands
201 11 (SWIR wavelength = 1.610 μm), 8 (NIR wavelength=0.842 μm) and 4 (RED wavelength = 0.665 μm) provide
202 information about the severity of the fire; burn with high severity present a dark (low albedo) red/brown color
203 (Figure 1). We included the histogram of dNBR ($\text{NBR}_{\text{postfire}} - \text{NBR}_{\text{prefire}}$) for the 317 training points labelled
204 ‘burned’ in Supplementary Figure S2 to corroborate that the ‘burned’ training samples were selected in areas with
205 medium to high severity fires. Eighty one percent (256) of ‘burned’ training points (317) had dNBR values
206 ($\text{NBR}_{\text{postfire}} - \text{NBR}_{\text{prefire}}) < -0.44$, which represents the threshold for medium to high severity burns according to the
207 proposed classification table of the United States Geological Survey (USGS).

208

209 *2.4. Burned-area map validation.*

210 The Gold standard is to validate the map against a sufficiently large reference dataset developed based on ground
211 visits to ‘burned’ and ‘unburned’ sites sampled objectively and randomly across the region of interest (Olofsson
212 et al. 2014). We sought alternative ways to generate the reference dataset because the sample of GPS locations of
213 ‘burned’ locations collected by Indonesian government were not available. Given the laborious scale of this
214 validation exercise, we validated our burned-area estimates for only the seven provinces prioritized by the

215 Indonesian Government for restoration of fire-prone degraded lands (Kalimantan Barat, Kalimantan Tengah and
216 Kalimantan Selatan, Papua, Jambi, Riau, and Sumatra Selatan). These provinces are also those that typically burn
217 most extensively. We used visual interpretations of the original time-series Sentinel-2 imagery acquired every 5
218 days over 2019 at 1298 randomly selected sites (one site = one pixel of 20 m x 20 m) to detect flaming fronts (fire
219 hotspots) and other signs of burning (smoke and charred vegetation). We used these reference data to calculate
220 the overall accuracy (OA), producer's accuracy (PA), and user's accuracy (UA) with a 95% confidence interval,
221 of all three burned area maps (i.e., our Sentinel-derived burned-area classification, the official Landsat-based
222 burned-area map, and the MCD64A1 product) following "good practices" for estimating area and assessing
223 accuracy reported by Olofsson et al. 2014. We use the term '*mapped burned-area*' for the area classified as burned
224 by each burned-area map. We employ the term '*corrected burned-area*' for the estimation of the burned area
225 based on the validation of a given burned-area map against the reference dataset, following the practices in
226 Olofsson et al. 2014. For instance, a high omission rate in the 'burned' class of a given burned-area estimate would
227 potentially lead to a lower *mapped area* than a *corrected area* for that estimate, while a high commission rate
228 would potentially lead to a higher *mapped area* than the *corrected area*. The *corrected area* represents an
229 estimation of the actual burned area for year 2019 computed for each of the three datasets separately. The accuracy
230 of the burned area map, and the sample size of the reference dataset, play a role in the confidence interval of
231 *corrected area* estimate. Lower map accuracy and smaller sample size mean wider confidence intervals.

232

233 2.4.1. Reference site sampling design

234 Good practices for estimating area and assessing accuracy, as reported in Olofsson et al. (2014), assumes a simple
235 random sampling or a stratified random sampling in the generation of the reference dataset. In our case study, we
236 employed a stratified-random sampling approach to ensure an acceptable sample of 'burned' reference sites. Our
237 stratified approach was necessary given that the 'burned' class was rare over the study area: the area of seven
238 provinces of interest is 87.6 Mha and the combined area detected as burned by all three datasets represented only
239 3.1% of this area.

240 For the generation of the 1298 reference sites (see Supplementary Table S4 for associated landcover types one
241 year before fire), we randomly sampled (i) 419 sites across from the areas classified 'burned' by the three datasets
242 (red area in Figure 3a; Supplementary Table S2), and (ii) 879 sites in areas classified as 'unburned' by all three
243 datasets hereafter denoted U (grey area in Figure 3a). This sample size is deemed sufficient and comparable to
244 other map assessments at larger scale (Stehman et al., 2003; Olofsson et al., 2014).

245 This initial sample of 1298 total sites present a shortcoming for direct pair-wise comparisons of between the
246 reference dataset and each of the three burned-area maps individually. Specifically, sampling densities in the
247 reference dataset were far greater in areas classified 'burned' by the three datasets (red area in Figure 3a) compared
248 to the area deemed 'unburned' by all three datasets, hereafter denoted U (grey area in Figure 3a). Consequently,
249 for the validation of a given burned-area dataset, its total number of 'unburned' reference sites would be over-
250 sampled upon defining 'unburned' reference sites with reference to U as well as areas classified as burned uniquely
251 by one of the other two maps (cyan areas in Figure 3b, c, d, hereafter denoted as U'). Such over-sampling of
252 reference sites in the realm of U' would violate the stratified-sampling approach described in Olofsson et al.
253 (2014) and would lead to an erroneous accuracy assessment. To achieve a balanced stratified sampling of reference
254 sites across 'burned' and 'unburned' areas of each dataset, we generated three subsamples from the initial 1298

255 reference sites (red areas in Figures 3e,f,g) and used these subsamples to validate each dataset. These three
256 subsamples were generated by randomly excluding reference sites from the realm of U' in Figure 3b, c and d,
257 respectively, until the density of reference sites in U' equaled the density of the larger unburned area U. For
258 instance, for the validation of the Official burned-area map, the density of reference sites in U was 10.36 sites/Mha,
259 and the extent of U' was 1.551 Mha, such that the number of reference sites to retain in U' for this validation was
260 given as 1.551 Mha x 10.36 sites/Mha =16 sites. The calculations of the number of sites removed from each
261 subsample are illustrated in Supplementary Table S3. The final, adjusted, stratified subsamples of reference sites
262 used for validation is given in Table 1.

263 2.4.2. Interpretation of the burned-area reference dataset

264 We developed a series of scripts in the Google Earth Engine to streamline the visual interpretation of the reference
265 sites. Specifically, we adapted a script written by (Olofsson et al. 2014) to rapidly scan the time-series of original
266 Sentinel-2 images in visible and infrared bands and thus visually detect either a smoke plume, a burn, or a heat
267 source (flaming front), and determine whether and when in 2019 a reference site burned. The script enabled the
268 interpreter to interactively track the evolution of NBR values and patterns over the 2019 time series of 5-day
269 images. Reference sites were investigated for burning wherever a marked drop in the NBR time series was
270 detected, indicating a disturbance in the vegetation. For reference sites where a disturbed area was observed, we
271 subsequently reviewed the last few images before the drop in NBR and the first few images after the drop.
272 Interpreters looked for three distinct signs of burning in these images to confirm them as burned: (i) smoke plumes;
273 (ii) flaming fronts – that is, a line a moving fire where the combustion is primarily flaming; and (iii) rapid changes
274 in color from 'green' to 'dark red', characteristic of a transition to charred vegetation (Figure 4). If rapid changes
275 in color were observed over the reference site, with at least one direct feature (smoke or flame) in its vicinity, this
276 indicated a fresh burn, and the reference site was declared 'burned'. If rapid changes in color from 'green' to 'dark
277 red' were observed without smoke or flame, the reference site was also declared 'burned'. If no change in color
278 was observed, with at least one direct feature (smoke or flame) in its vicinity, the reference site was declared
279 'unburned'. If none of these three features were observed, the reference site was declared 'unburned'.

280

281 Three interpreters independently reviewed the time-series of original Sentinel-2 images and associated NBR
282 trends for all reference sites (N=1298) (see Supplementary Figure S3 for a frequency distribution of burn sizes of
283 the Sentinel-2 burned-area map, for select spatially coincident 'burned' reference sites). To reduce uncertainties
284 associated with the interpretation of the imagery, the results of the three interpreters were compared to each other.
285 If all three interpreters recorded the same interpretation and timing of a burning event for a given reference site,
286 their interpretations were retained. If one or more interpreters disagreed, all interpreters reviewed the data and
287 resolved discrepancies by consensus. In some cases, it was difficult to reconcile disagreements because of poor
288 image quality or because of uncertain spectral patterns. Therefore, if possible, interpreters also explored other
289 satellite images (e.g. Landsat) to detect the presence of fire and resolve disagreements for a given reference site.
290 The sites in which the three interpreters disagreed were ultimately excluded (70 sites) from the reference dataset.
291 For these excluded sites, disagreement typically resulted from uncertainties over the boundary of burned or
292 unburned areas, or because the imagery was not clear enough. The sample size of reference points explored here,
293 N=1298, excludes the discarded points of disagreement in question.

294 We created a second script to generate snapshot images (see examples in Figure 4) depicting infrared spectral
295 conditions, shortly before and shortly after a fire, as well as the corresponding image dates. Interpreters recorded

296 and geotagged a snapshot of before and after fire condition at every reference site (for which a burned area was
297 detected) to enable third-party reviewers to check the consistency and validity of interpretations on site-by-site
298 basis (See Data Availability).

299

300 2.4.3. *Burn size comparisons.*

301 We tested whether, and how, the three burned-area estimates differed in their tendencies to incorporate burns of
302 larger or smaller sizes. Specifically, we compared the frequency distributions of burn areas (or “scars”) amongst
303 the three estimates to test for similarity and qualify any distinguishing differences on the part of our Sentinel-
304 based estimate. Differences amongst burn size frequency distributions implies that a given burned-area estimate
305 is inclusive of burn of a given size, regardless of absolute differences to total burned area between the estimates.
306 Inter-estimate comparisons of burn-scar size frequency is analogous to tests of whether the ‘samples’ of burns
307 defined by each estimate describe the same, ultimately partially-observed universe of fire activity. Significant
308 inter-estimate differences imply greater or lesser inclusion of a given realm of fire activity – e.g., small-scale
309 agricultural burning, plantation fires, extreme wildfires – thus indicating bias (or lack thereof) without defining
310 such realms explicitly.

311 For all three estimates, we employed the Kruskal-Wallis H test of differences with respect to the ‘location’ of
312 frequency distributions along a continuum of burn sizes. Given significant inter-estimate differences according
313 to this three-way test, we tested for two-way differences in the shape and location of the burn-size frequency
314 distribution (Kolmogorov-Smirnov test), as well as two-way differences in medians (Mann-Whitney U test),
315 between our Sentinel estimate and either the Official or MODIS estimate individually. Testing for similarity over
316 increasingly large scar-size cohorts clarified the degree to which significant inter-estimate differences were
317 attributable to the inclusion or omission of a given cohort.

318 We excluded burns <6.25 ha because this is the minimum observable burn-size of the Landsat-8 Official estimates
319 due to the challenging nature of visual interpretations at such scales. We note that the minimum size of the MODIS
320 data is 25 ha, hence for comparison with MCD64A1 product we used a 25-ha threshold. In relation to Sentinel
321 and MODIS estimates, for which burned areas were originally mapped as arrays of pixels, we defined a burn to
322 be any array of pixels contiguous across cardinal directions but not diagonals to render the resultant burned-area
323 map conservative with respect to patch size (Figure S4). For the Official estimate, burns are as manually
324 delineated via visual interpretation by interpreters from the Government of Indonesia. All burns are spatially and
325 temporally discrete, such that burns of a given estimate that overlap spatially but not temporally are considered
326 separate.

327

328 3. Results

329

330 3.2. *Increased Burned-Area Estimates*

331 Our Indonesia-wide burned-area estimate, based on the classification of the pair of pre- and post-fire Sentinel-2
332 composites, are larger than the Official estimates as well as the MODIS MCD64A1 to a lesser degree. We estimate
333 3.11 million hectares (Mha) burned in 2019 across Indonesia, of which 31% were on peat (Figure 5). The extent
334 of peatlands were defined using a national dataset from the Ministry of Agriculture (Ritung et al., 2011). In

335 contrast, Official burned-area estimates, based on visual interpretation of Landsat-8 imagery, report only about
336 half as much burned area, at 1.64 Mha, of which 39% was on peat. Our estimates too are greater than the MODIS
337 MCD64A1 product, which reports 2.04 Mha burned in 2019, or two-thirds of our estimate, with 40% on peat.
338 The greater burning extent and proportionally lesser extent of peatland burning according to our estimates suggest
339 that our estimates are particularly more inclusive of burning across mineral soils.

340 In the seven provinces for which we assessed accuracy, our Sentinel-2 estimates, and the Official Landsat-8
341 estimates both report excellent user's accuracies (UA) for the 'burned' class, at 97.9% (CI: 97.1%-98.8%) and
342 95.1% (CI: 93.5%-96.7%) respectively, indicating a mere 2.9%-4.9% commission-error rate (Table 2,
343 Supplementary Table S5). The producer's accuracies (PA) are comparatively lower for both datasets, but notably
344 less so for our estimates, at 75.6% (CI: 68.3%-83.0%) and 49.5% (CI: 42.5%-56.6%) for our estimate and the
345 Official dataset, respectively. In other words, for any burned area in our reference dataset, there is a 75.6% chance
346 that it will be correctly mapped as burned by our estimate, compared to only a 49.5% for the official estimate.
347 This is in keeping with the greater tendency of the Sentinel-2 estimate to capture more smaller and intermediate-
348 size burns. The MCD64A1 data had a much lower UA for the burned class, at 76.0% (CI: 73.3%-78.7%), as well
349 as a much lower and a PA for the burned class, at 53.1% (CI: 45.8%-60.5%), qualifying it as the least reliable and
350 accurate of the three estimates notwithstanding comparable high overall accuracy (Table 2).

351 All three burned-area maps underestimate the true burned area extent, as per their respective PA figures, but our
352 Sentinel-based map has the smallest shortfall and also maintains user accuracy. The corrected burned area of the
353 seven provinces is higher than the mapped area for all the three burned area maps. Again, however, our map area
354 most closely approximates its corresponding corrected burned area (Table 2). Whereas our Sentinel-based mapped
355 burned area indicates that 1.84 Mha burned in the seven provinces (or 59% of our total national estimated burned
356 area), the corrected burned area is 2.38 Mha (CI: 2.14 Mha-2.61 Mha) (Table 2), for a discrepancy of 0.54 Mha.
357 In contrast, the official estimate indicates 1.19 Mha burned in the seven provinces (73% of its corresponding
358 total), and a corrected burned area of 2.29 Mha (CI: 1.96 Mha-2.63 Mha), for a 1.1 Mha discrepancy. Likewise,
359 the MCD64A1 dataset mapped 1.58 Mha burned in the seven provinces and has a corrected burned area of 2.27
360 Mha (CI: 1.94 Mha-2.59 Mha), for a 0.69 Mha discrepancy. Although, we cannot extrapolate a corrected burned
361 area across Indonesia, we are confident that more than 3.11 Mha burned in 2019.

362 *3.1. Burn size comparison.*

363 The Sentinel, Official and MCD64A1 estimates captured significantly distinct realms of fire activity, as
364 represented by relative burn size frequencies (Figure S6). The three estimates differ from one another most
365 notably for small burns, however, they are statistically indistinguishable for burns > 5000 ha indicative of extreme
366 fire activity (Table 3). In other words, all three estimates capture very large burns (>5000 ha) equally well, and
367 distinctions amongst the estimates concentrate amongst small (<100 ha), intermediate (100-1000 ha) and larger
368 burns (1000-5000 ha), in decreasing order of degree as indicated by the magnitude of the test statistics in Table 3.

369 Inclusivity of smaller and intermediate burned areas is the primary source of difference among estimates.
370 Compared to Official or MCD64A1 estimates, the Sentinel estimate has a significantly greater relative frequency
371 of small burned areas (< 100 ha), especially amongst the smallest of these (Table 4). This is indicative of a greater
372 detection of small fires presumably characterized by small-scale agriculture fires and similar, small-scale
373 controlled burning. The Sentinel estimate similarly has a greater relative frequency of intermediate sized burns
374 (100-1000 ha), but less acutely so, with inter-estimate differences being more moderate for the Official estimate

375 than the MCD64A1 estimate (Table 4, Figure 6, Figure S6). For burns >1000 ha, the Sentinel estimate differs
376 only relative to the official estimate (Table 3), seemingly due to the latter's underestimation of large and very
377 large scars (Figure 6). Note for instance the increasingly large divergence between the cumulative burned-area
378 curves for the Sentinel-2 and the Official estimates in Figure 6 for burn areas > 1000 ha. For very large burns (>
379 5000 ha), two-way comparisons in Table 4 again report no significant statistical differences in burn-scar detection
380 rates between the Sentinel and alternative estimates. However, given the small sample of patches > 5000 ha, it is
381 noteworthy that the Sentinel estimate captures more very large scars compared to Official estimates (n=56 vs
382 n=16) and avoids critical omissions made by both Official, or MCD64A1, estimates for extremely large burns
383 (>15,000 ha) on peatlands around Berbak National Park in Jambi Province, Sumatra (Figure 7).

384 In summary, the greater overall burned-area estimate of our Sentinel data compared to the Official and MCD64A1
385 alternatives reflects differences in the inclusion of smaller and intermediately sized scars. The sum of all Sentinel
386 burn areas that are individually <~860 ha equals the entirety of the official burned-area estimate (Figure 6). The
387 Sentinel-2 data exhibit a size-frequency pattern that approximates a near scale-free power-law (Figure 6).

388 **4. Discussion**

389 We developed a method that generates two national composite Sentinel-2 images depicting vegetation condition
390 before and after burning in 2019 (Figure 1), and then classified this pair to extract burned areas using a Random
391 Forest supervised classification algorithm. We developed a comprehensive validation protocol to strictly assess
392 the reliability and accuracy of our product based on visual interpretation of dense time-series Sentinel-2 original
393 images, and also applied this validation to the widely used global MODIS burned-area product (MCD64A1,
394 collection 6) (Giglio et al., 2018) and to the Official burned-area product of the Indonesian Ministry of
395 Environment and Forestry (MOEF) (Sipongi, 2020).

396 Our estimate is the most reliable and accurate and therefore captures more of the 2019 total burned area,
397 confirming that 20-m Sentinel-2 imagery is better suited to widespread small-scale burning in Indonesia (Huang
398 et al., 2016), while it also captures large burn scars relatively thoroughly. The study finds similar omission and
399 commission errors (47% and 24%) for the 'burned' class of MCD64A1 product as those presented globally (40%
400 and 22%) (Giglio et al., 2018). The underestimation of total burned area according to the MCD64A1 product
401 compared with our Sentinel-2 estimate is unsurprising, considering that the MODIS 500-m pixel resolution
402 struggles to detect smaller fires (Giglio et al., 2018). Similar conclusions were reached by Ramo et al. (2021)
403 when comparing the new 'Small Fire Dataset' derived using Sentinel-2 over Sub-Saharan Africa (Chuvienco et al.,
404 2018) and the MCD64A1 product. More surprising is the near 2:1 ratio by which the Sentinel-2 estimates surpass
405 the Landsat-8 Official estimate. Our examination shows that this difference reflects differential detection of small-
406 (<100 ha) to intermediate-sized (<1000 ha) burn scars.

407 The Sentinel-2 data exhibit a size-frequency pattern that approximates closer to a near scale-free power-law, or
408 pareto distribution (Karsai et al., 2020; Falk et al., 2007). These patterns are typical of large-scale fire studies
409 (Malamud et al., 1998). Both other methods yield an S-shaped curve with less area at smaller and larger sizes than
410 captured in the Sentinel-2, indicating likely bias by omission over the entire range of scales and are not determined
411 by image resolution alone (Figure 6). These results, with different frequency patterns arising from burns from the
412 same regions in the same period, also highlight the danger in interpreting apparent burned-area patterns without
413 careful consideration of the limitations and biases that arise from the methods used to map them—an issue that
414 may not have always been sufficiently recognized in past assessments or policy.

415 Although both Sentinel-2 and Landsat-8 both observe the infrared wavelengths required to detect charred
416 vegetation and have similar spatial resolutions (20 m x 20 m and 30 m x 30 m, respectively), Sentinel-2 detects
417 more burns of the greater frequency of its coverage (five- versus sixteen-day revisit time). Also, our method
418 avails of the massive computational capabilities and automation of the Google Earth Engine, allowing us to
419 analyze more images and thus map more and smaller burn scars and associated details than could even the most
420 well-equipped team of visual interpreters.

421 Despite high reliability that every burn scar detected on the map was valid (2.9% commission error rate), our
422 method suffered a 24.4% omission error rate (burned areas that remained undetected). These rates reflect
423 necessary tradeoffs between commission and omission error in a context where conservative estimates are much
424 preferred for environmental policy and monitoring. We prioritized a low commission error rate (i.e. high user's
425 accuracy) over absolute burned-area coverage to address sensitivities (Rochmyaningsih, 2020). By hedging
426 against commission errors, our approach omitted hard-to-detect events, including low-intensity burns, such as
427 those that occur beneath the forest canopy on mineral soils (van Nieuwstadt and Sheil, 2005) or on savanna
428 grasslands, which tend to re-green rapidly. While further work is required to clarify and refine the optimal levels
429 of inclusivity and reliability, we emphasize that the production of before and after fire annual composite images
430 is relatively straightforward for the user community, given the availability of both the necessary imagery and our
431 Google Earth Scripts.

432 While the accuracy assessment proved that our training dataset is valid for the classification of Sentinel-2
433 composites for the year 2019 in Indonesia, this training dataset might not achieve equivalent accuracy for other
434 years and regions. The pre- and post-fire composites might show different spectral changes under different
435 conditions. For instance, high rainfall in 2020 influenced reflectance. Similarly, representative training points
436 should be used in other regions. Those adapting these methods should ensure adequate local training data and
437 validation.

438 Doubts may persist concerning confident estimates of burn areas without extensive and costly ground-checks.
439 Modern high-resolution remote sensing makes such on-the-ground checks less essential than in the past as burned
440 areas are readily identified with good accuracy in modern high-resolution imagery such as that we used for our
441 validation. The protocol developed here to generate a reference dataset based on visual inspection of dense (5-day
442 revisit time) satellite imagery is better suited than ground verifications of 'burned' and 'unburned' locations,
443 because it allows the generation of extensive randomly distributed well characterised reference sites, a process
444 too time-consuming and costly with field visits. The identification and quantification of less-readily-detected
445 burned areas, such as those under a closed forest canopy, remain a challenge but will require dedicated and
446 targeted research and would not be solved by ground-checks alone.

447 Accurate estimates of burned lands, in particular on peat, are central to addressing concerns about regional air
448 quality, and to ambitious national climate-change atmospheric carbon reduction commitments heavily reliant on
449 improved land/fire management (DGCC, 2019). Though we observed proportionally less peatland burning than
450 the alternative burned-area estimates (31% versus 39% and 40% for the Official and MCD64A1 products,
451 respectively), due to our more complete coverage, we observed more peatland burning absolutely (0.96 Mha) than
452 the official estimate (0.64 Mha). Given this large discrepancy for peatland burning, we anticipate that our refined
453 burned area product will enable others to better estimate carbon emissions from the 2019 fires in Indonesia.
454 Combined with daily fire hotspots detected using thermal remote sensing, our detailed burned-area map can help

455 identify ignition sites and estimate fire duration more precisely, and therefore contribute to forensic analyses of
456 burning across landholdings (Gaveau et al., 2017) as well as assess policies and practices intended to reduce or
457 control ignition events and the scale of fires (Watts et al., 2019).

458 The Indonesian government has shown some success in reducing fires (Sloan et al., 2021). Apparent reductions
459 to fire activity would however ideally be qualified using our more inclusive and accurate burned-area estimates.
460 Further, the Indonesian government must also develop improved protocols to quantify the resulting carbon
461 emissions (DGCC, 2019). Our protocols for creating reliable pre- and post-fire composites are replicable. To
462 further the adoption and reproduction of our approach, we have published all our protocols, scripts, applications,
463 burned-area map, reference data, pre-fire and post-fire Sentinel-2 composite images, and various other outputs so
464 that anyone may employ and revise them as they wish (see Data Availability).

465

466 **5. Code availability**

467 The code that generates the Sentinel-2 pre- and post-fire composites can be found at:
468 https://github.com/thetreemap/IDN_annual_burned_area_detection

469 **6. Data Availability**

470 All the data including pre- and post-fire composites, all three burned area products, and reference points with
471 screenshots can be visualized online at this application portal:
472 <https://thetreemap.users.earthengine.app/view/burn-area-validation-simplified>

473 The Sentinel-based burned area map and reference dataset are freely available for download at:
474 <https://doi.org/10.5281/zenodo.4551243> (Gaveau et al., 2021).

475 The dataset *2019_burnedarea_indonesia.shp* contains the 2019 burned-area estimates that we developed for
476 Indonesia using 20 m x 20 m time-series Sentinel-2 imagery. The reference dataset *Reference_dataset.shp*
477 contains 1298 reference points that we assembled and used to validate all three burned area products described in
478 this study. Each reference point includes attribute 'REFERENCE' to describe the values obtained by visual
479 interpretation: either 'NO' unburned or 'YES' burned. Each reference point has three attributes: 'C_SENTINEL'
480 'C_OFFICIAL' and 'C_MCD64A1' to describe the values of the classification of each burned area product: either
481 'NO' unburned or 'YES' burned. Finally, each reference point has three additional attributes: 'SENTINEL',
482 'OFFICIAL', and 'MCD64A1' to describe which burned area product this reference point validates. The values
483 are either 0: not validate or 1: validate.

484 The MODIS MCD64A1 dataset was obtained at: [https://developers.google.com/earth-
485 engine/datasets/catalog/MODIS_006_MCD64A1](https://developers.google.com/earth-engine/datasets/catalog/MODIS_006_MCD64A1). The official burned area dataset from the Ministry of
486 Environment and Forestry (MOEF) was obtained at: <https://geoportal.menlhk.go.id/webgis/index.php/en/>

487 The Sentinel-2 Level 2A used in this study are available at <https://scihub.copernicus.eu/> and can be retrieved in
488 Google Earth Engine. The Sentinel- 2 data are hosted and accessed in the Earth Engine data catalog (the links to
489 the data are https://developers.google.com/earth-engine/datasets/catalog/COPERNICUS_S2_SR). Data ingested
490 and hosted in Google Earth Engine are always maintained in their original projection, resolution, and bit depth
491 (Gorelick et al., 2017).

492

493 **Financial support.** Funding by the CGIAR Research Program on Forests, Trees and Agroforestry (CRP-FTA),
494 with financial support from the donors to the CGIAR Fund, is recognized.

495

496 **Author Contributions.** D.L.A.G. designed the study. D.L.A.G, M.A.S. and A.D designed the burn scar detection
497 method. M.A.S. and A.D wrote the code in Google Earth Engine. D.L.A.G, M.A.S. and A.D. carried out the
498 validation. S.S. carried out the burn scar size analysis. D.L.A.G., A.D. S.S. and D.S. interpreted the results and
499 wrote the manuscript and produced the figures.

500

501 **Competing interests.** The authors declare no competing interests. Readers are welcome to comment on the online
502 version of the paper.

503

504 **References**

505 Adrianto, H. A., Spracklen, D. V., Arnold, S. R., Sitanggang, I. S., and Syaufina, L.: Forest and Land Fires Are
506 Mainly Associated with Deforestation in Riau Province, Indonesia, *Remote Sensing*, 12, 3, 2020.

507

508 Alonso-Canas, I., and Chuvieco, E.: Global burned area mapping from ENVISAT-MERIS and MODIS active fire
509 data, *Remote Sensing of Environment*, 163, 140-152, 2015.

510

511 Breiman, L.: Random forests, *Machine learning*, 45, 5-32, 2001.

512

513 Cai, W., Yang, K., Wu, L., Huang, G., Santoso, A., Ng, B., Wang, G., and Yamagata, T.: Opposite response of
514 strong and moderate positive Indian Ocean Dipole to global warming, *Nature Climate Change*, 11, 27-32,
515 10.1038/s41558-020-00943-1, 2021.

516

517 Carmenta, R., Zabala, A., Trihadmojo, B., Gaveau, D., Salim, M. A., and Phelps, J.: Evaluating bundles of
518 interventions to prevent peat-fires in Indonesia, *Global Environmental Change*, 102154, 2020.

519

519 Cochrane, M. A.: Fire science for rainforests, *Nature*, 421, 913-919, 2003.

520

521 Chuvieco, E., Mouillot, F., van der Werf, G. R., San Miguel, J., Tanase, M., Koutsias, N., García, M., Yebra, M.,
522 Padilla, M., and Gitas, I.: Historical background and current developments for mapping burned area from satellite
523 Earth observation, *Remote Sensing of Environment*, 225, 45-64, 2019.

524

525 Chuvieco, E.; Pettinari, M.L.; Bastarrika, A.; Roteta, E.; Storm, T.; Padilla Parellada, M.: ESA Fire Climate
526 Change Initiative (Fire_cci): Small Fire Dataset (SFD) Burned Area pixel product for Sub-Saharan Africa, version
527 1.1. Centre for Environmental Data Analysis, 12 October 2018, 2018.
528 doi:10.5285/065f6040ef08485db989cbd89d536167.

529

530 Crippa, P., Castruccio, S., Archer-Nicholls, S., Lebron, G., Kuwata, M., Thota, A., Sumin, S., Butt, E.,
531 Wiedinmyer, C., and Spracklen, D.: Population exposure to hazardous air quality due to the 2015 fires in
532 Equatorial Asia, *Scientific reports*, 6, 1-9, 2016.

533

534 Dennis, R. A., Mayer, J., Applegate, G., Chokkalingam, U., Colfer, C. J. P., Kurniawan, I., Lachowski, H., Maus,
535 P., Permana, R. P., and Ruchiat, Y.: Fire, people and pixels: linking social science and remote sensing to
536 understand underlying causes and impacts of fires in Indonesia, *Human Ecology*, 33, 465-504, 2005.

537

538 DGCC: Emission Reduction Report, Directorate General of Climate Change, 2019.

539

540 Falk, D. A., Miller, C., McKenzie, D., and Black, A. E.: Cross-scale analysis of fire regimes, *Ecosystems*, 10,
541 809-823, 2007.

542

543 Fanin, T., and Werf, G. R.: Precipitation–fire linkages in Indonesia (1997–2015), *Biogeosciences*, 14, 3995–4008,
544 2017.

545

546 Field, R. D., van der Werf, G. R., and Shen, S. S.: Human amplification of drought-induced biomass burning in
547 Indonesia since 1960, *Nature Geoscience*, 2, 185–188, 2009.

548

549 Field, R. D., Van Der Werf, G. R., Fanin, T., Fetzer, E. J., Fuller, R., Jethva, H., Levy, R., Livesey, N. J., Luo,
550 M., and Torres, O.: Indonesian fire activity and smoke pollution in 2015 show persistent nonlinear sensitivity to
551 El Niño-induced drought, *Proceedings of the National Academy of Sciences*, 113, 9204–9209, 2016.

552

553 Fletcher, K.: SENTINEL 2: ESA's Optical High-Resolution Mission for GMES Operational Services, European
554 Space Agency, 2012.

555

556 Gaveau, D.L.A, Salim, M, Hergoualc'h, K, Locatelli, B, Sloan, S, Wooster, M, Marlier, M, Molidena, E, Yaem,
557 H, Defries, R, Verchot, L, Murdiyarso, D, Nasi, R, Holmgren, P & Sheil, D.: Major atmospheric emissions from
558 peat fires in Southeast Asia during non-drought years: evidence from the 2013 Sumatran fires. *Scientific Reports*
559 4:6112, 2014.

560

561 Gaveau, D. L.A, Pirard, R., Salim, M. A., Tonoto, P., Parks, S. A., and Carmenta, R.: Overlapping land claims
562 limit the use of satellites to monitor No-Deforestation commitments and No-Burning compliance, *Conservation*
563 *Letters*, 2017.

564

565 Gaveau, D. L.A, Descal, A, Salim, M.A, Sheil, D, & Sloan, S. 2019 burned area map for Indonesia using Sentinel-
566 2 data [Data set]. Zenodo. <https://doi.org/10.5281/zenodo.4551243>, 2021.

567

568 Gaveau, D. L.A, Santos, L., Locatelli, B., Salim, M. A., Husnayaen, H., Meijaard, E., Heatubun, C., and Sheil,
569 D.: Forest loss in Indonesian New Guinea (2001–2019): Trends, drivers and outlook, *Biological Conservation*,
570 261, 109225, 2021.

571

572

573 Giglio, L., Boschetti, L., Roy, D. P., Humber, M. L., and Justice, C. O.: The Collection 6 MODIS burned area
574 mapping algorithm and product, *Remote sensing of environment*, 217, 72–85, 2018.

575

576 Gorelick, N., Hancher, M., Dixon, M., Ilyushchenko, S., Thau, D., and Moore, R.: Google Earth Engine:
577 Planetary-scale geospatial analysis for everyone, *Remote Sensing of Environment*, 202, 18–27, 2017.

578

579 Harrison, M. E., Ripoll Capilla, B., Thornton, S. A., Cattau, M. E., and Page, S. E.: Impacts of the 2015 fire season
580 on peat-swamp forest biodiversity in Indonesian Borneo, *Peatlands in harmony–Agriculture, industry & nature*.
581 *Proceedings of the 15th international peat congress: Oral presentations*, 2016, 713–717,

582

583 Hawbaker, T.J., Vanderhoof, M.K., Beal, Y.-J., Takacs, J.D., Schmidt, G.L., Falgout, J.T., Williams, B., Fairaux,
584 N.M., Caldwell, M.K., Picotte, J.J., Howard, S.M., Stitt, S., Dwyer, J.L., 2017b. Mapping burned areas using
585 dense time-series of Landsat data. *Remote Sensing of Environment* 198, 504–522.

586

587 Huang, H., Roy, D. P., Boschetti, L., Zhang, H. K., Yan, L., Kumar, S. S., Gomez-Dans, J., and Li, J.: Separability
588 analysis of Sentinel-2A Multi-Spectral Instrument (MSI) data for burned area discrimination, *Remote Sensing*, 8,
589 873, 2016.

590

591 Huijnen, V., Wooster, M., Kaiser, J., Gaveau, D., Flemming, J., Parrington, M., Inness, A., Murdiyarso, D., Main,
592 B., and Van Weele, M.: Fire carbon emissions over maritime southeast Asia in 2015 largest since 1997, *Scientific*
593 *reports*, 6, 26886, 2016.

594

595 Karsai, I., Schmickl, T., and Kampis, G.: Forest Fires: Fire Management and the Power Law, in: *Resilience and*
596 *Stability of Ecological and Social Systems*, Springer, 63–77, 2020.

597

598

599

600 Koplitz, S. N., Mickley, L. J., Marlier, M. E., Buonocore, J. J., Kim, P. S., Liu, T., Sulprizio, M. P., DeFries, R.
601 S., Jacob, D. J., and Schwartz, J.: Public health impacts of the severe haze in Equatorial Asia in September–
602 October 2015: demonstration of a new framework for informing fire management strategies to reduce downwind
603 smoke exposure, *Environmental Research Letters*, 11, 094023, 2016.

604
605 Liu, S., Zheng, Y., Dalponte, M., and Tong, X.: A novel fire index-based burned area change detection approach
606 using Landsat-8 OLI data, *European journal of remote sensing*, 53, 104-112, 2020.
607
608 Lizundia-Loiola, J., Otón, G., Ramo, R., and Chuvieco, E.: A spatio-temporal active-fire clustering approach for
609 global burned area mapping at 250 m from MODIS data, *Remote Sensing of Environment*, 236, 111493, 2020.

610 Lizundia-Loiola, J., Franquesa, M., Boettcher, M., Kirches, G., Pettinari, M. L., and Chuvieco, E.: Operational
611 implementation of the burned area component of the Copernicus Climate Change Service: from MODIS 250 m
612 to OLCI 300 m data, *Earth System Science Data Discussions*, 1-37, 2021.

613 Lohberger, S., Stängel, M., Atwood, E. C., and Siegert, F.: Spatial evaluation of Indonesia's 2015 fire-affected
614 area and estimated carbon emissions using Sentinel-1, *Global change biology*, 24, 644-654, 2018.
615
616 Malamud, B. D., Morein, G., and Turcotte, D. L.: Forest fires: an example of self-organized critical behavior,
617 *Science*, 281, 1840-1842, 1998.
618
619 Marlier, M. E., DeFries, R. S., Voulgarakis, A., Kinney, P. L., Randerson, J. T., Shindell, D. T., Chen, Y., and
620 Faluvegi, G.: El Niño and health risks from landscape fire emissions in southeast Asia, *Nature climate change*, 3,
621 131-136, 2013.

622
623 Olofsson, P., Foody, G. M., Herold, M., Stehman, S. V., Woodcock, C. E., and Wulder, M. A.: Good practices
624 for estimating area and assessing accuracy of land change, *Remote Sensing of Environment*, 148, 42-57,
625 <http://dx.doi.org/10.1016/j.rse.2014.02.015>, 2014.
626
627 Otón, G., Ramo, R., Lizundia-Loiola, J., and Chuvieco, E.: Global detection of long-term (1982–2017) burned
628 area with AVHRR-LTDR data, *Remote Sensing*, 11, 2079, 2019.
629
630 Ramo, R., Roteta, E., Bistinas, I., Van Wees, D., Bastarrrika, A., Chuvieco, E., and Van der Werf, G. R.: African
631 burned area and fire carbon emissions are strongly impacted by small fires undetected by coarse resolution satellite
632 data, *Proceedings of the National Academy of Sciences*, 118, 2021.
633
634 Ritung, S., Wahyunto, Nugroho, K., Sukarman, Hikmatullah, Suparto, and C, T.: Peatland map of Indonesia,
635 Department of Research and Development of Agricultural Land Resources, Ministry of Agriculture, 2011.
636
637 Rochmyaningsih, D.: Wildfire researcher deported amid growing rift between Indonesian government and
638 scientists, *Science*, 367, 722-723, 2020.
639
640 Sipongi.: Recapitulation of Land and Forest Fires Area (Ha) per Province in Indonesia 2015-2020:
641 [http://sipongi.menlhk.go.id/hotspot/luas kebakaran](http://sipongi.menlhk.go.id/hotspot/luas_kebakaran), 2020.
642
643 Sloan, S., Locatelli, B., Wooster, M. J., and Gaveau, D. L.: Fire activity in Borneo driven by industrial land
644 conversion and drought during El Niño periods, 1982–2010, *Global environmental change*, 47, 95-109, 2017.
645
646 Sloan, S., Tacconi, L., and Cattau, M.: Fire prevention in managed landscapes: Recent success and challenges in
647 Indonesia, *Mitigation and Adaptation Strategies for Global Change*, 26: Article 32, 2021.
648
649 Stehman, S. V., Wickham, J., Smith, J., and Yang, L.: Thematic accuracy of the 1992 National Land-Cover Data
650 for the eastern United States: Statistical methodology and regional results, *Remote Sensing of Environment*, 86,
651 500-516, 2003.
652
653 Tansey, K., Beston, J., Hoscilo, A., Page, S., and Paredes Hernández, C.: Relationship between MODIS fire hot
654 spot count and burned area in a degraded tropical peat swamp forest in Central Kalimantan, Indonesia, *Journal of*
655 *Geophysical Research: Atmospheres*, 113, 2008.
656
657 Van der Werf, G. R., Dempewolf, J., Trigg, S. N., Randerson, J. T., Kasibhatla, P. S., Giglio, L., Murdiyarso, D.,
658 Peters, W., Morton, D., and Collatz, G.: Climate regulation of fire emissions and deforestation in equatorial Asia,
659 *Proceedings of the National Academy of Sciences*, 105, 20350-20355, 2008.
660
661
662 Van Der Werf, G. R., Randerson, J. T., Giglio, L., Van Leeuwen, T. T., Chen, Y., Rogers, B. M., Mu, M., Van
663 Marle, M. J., Morton, D. C., and Collatz, G. J.: Global fire emissions estimates during 1997–2016, *Earth System*
664 *Science Data*, 9, 697-720, 2017.

665
666
667
668
669
670
671
672
673
674
675
676
677

678

679

680

681

682

683

684

685

686

687

688

689

690

691

692

693

694

695

696

697

698

699

van Nieuwstadt, M. G. L., and Sheil, D.: Drought, fire and tree survival in a Borneo rain forest, East Kalimantan, Indonesia, *Journal of Ecology*, 93, 191-201, 2005.

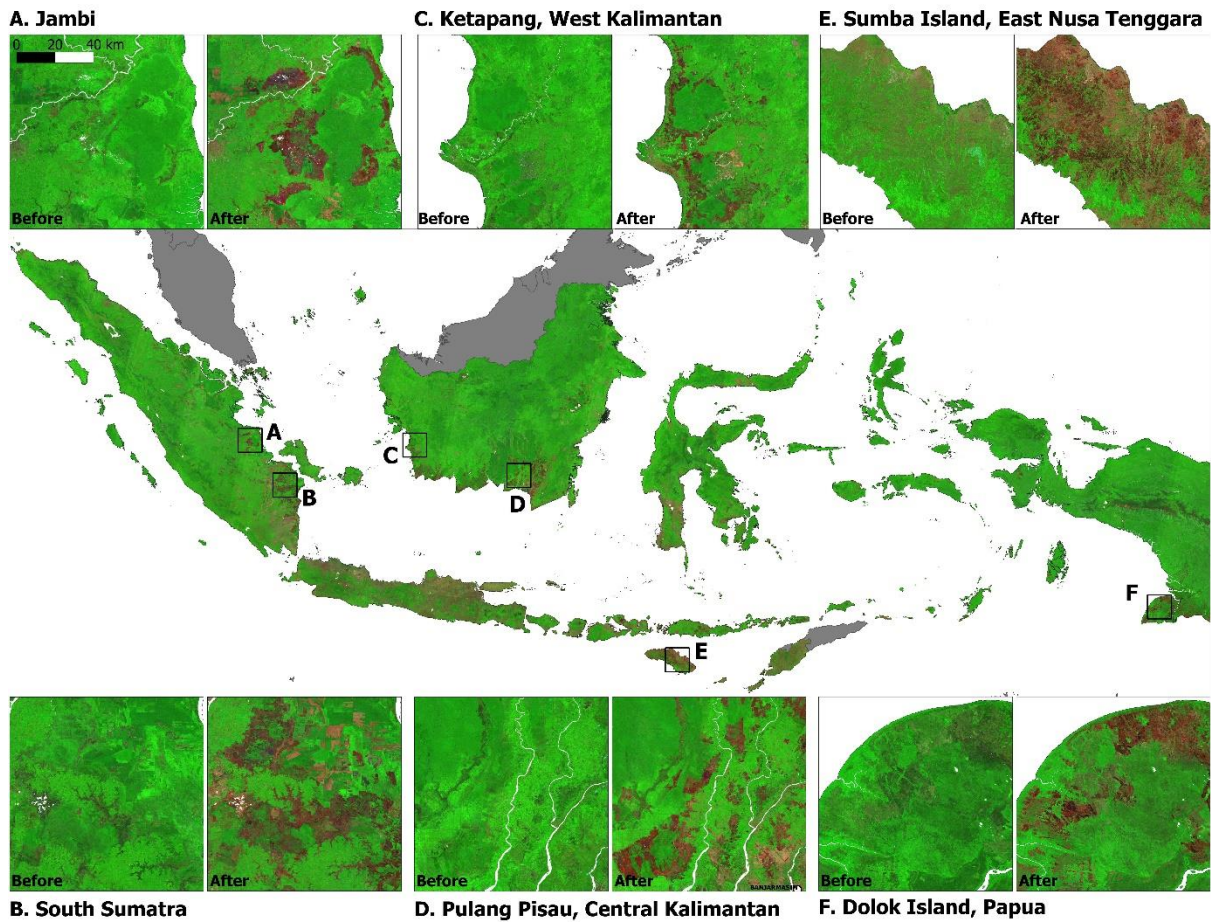
Watts, J. D., Tacconi, L., Hapsari, N., Irawan, S., Sloan, S., and Widiastomo, T.: Incentivizing compliance: Evaluating the effectiveness of targeted village incentives for reducing burning in Indonesia, *Forest Policy and Economics*, 108, 101956, 2019.

Wooster, M., Gaveau, D., Salim, M., Zhang, T., Xu, W., Green, D., Huijnen, V., Murdiyarso, D., Gunawan, D., and Borchard, N.: New tropical peatland gas and particulate emissions factors indicate 2015 Indonesian fires released far more particulate matter (but less methane) than current inventories imply, *Remote Sensing*, 10, 495, 2018.

700 **Figures**

701

702



703

704 **Figure 1.** The pair of cloud-free pre-and post-fire Sentinel-2 composites shown over six locations in insets A, B, C, D, E, F
705 (all insets have the same scale). The base Indonesia-wide imagery is the post-fire composite. Imagery displayed in false colors
706 (RGB: short-wave infrared (band 11); Near infrared (band 8), Blue: red (band 4)). In this pair of composite images acquired
707 shortly before and after fire a recently burned area will readily appear to have transitioned from 'green' to dark 'brown/red'
708 tones. Areas cleared without burning appear bright pink. Areas covered with vegetation appear dark to bright green.

709

710

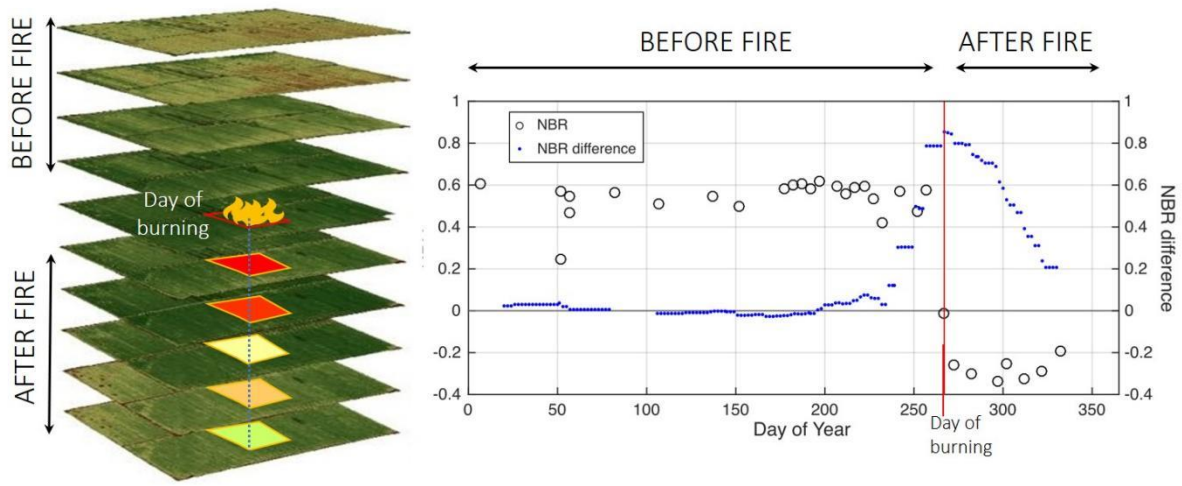
711

712

713

714

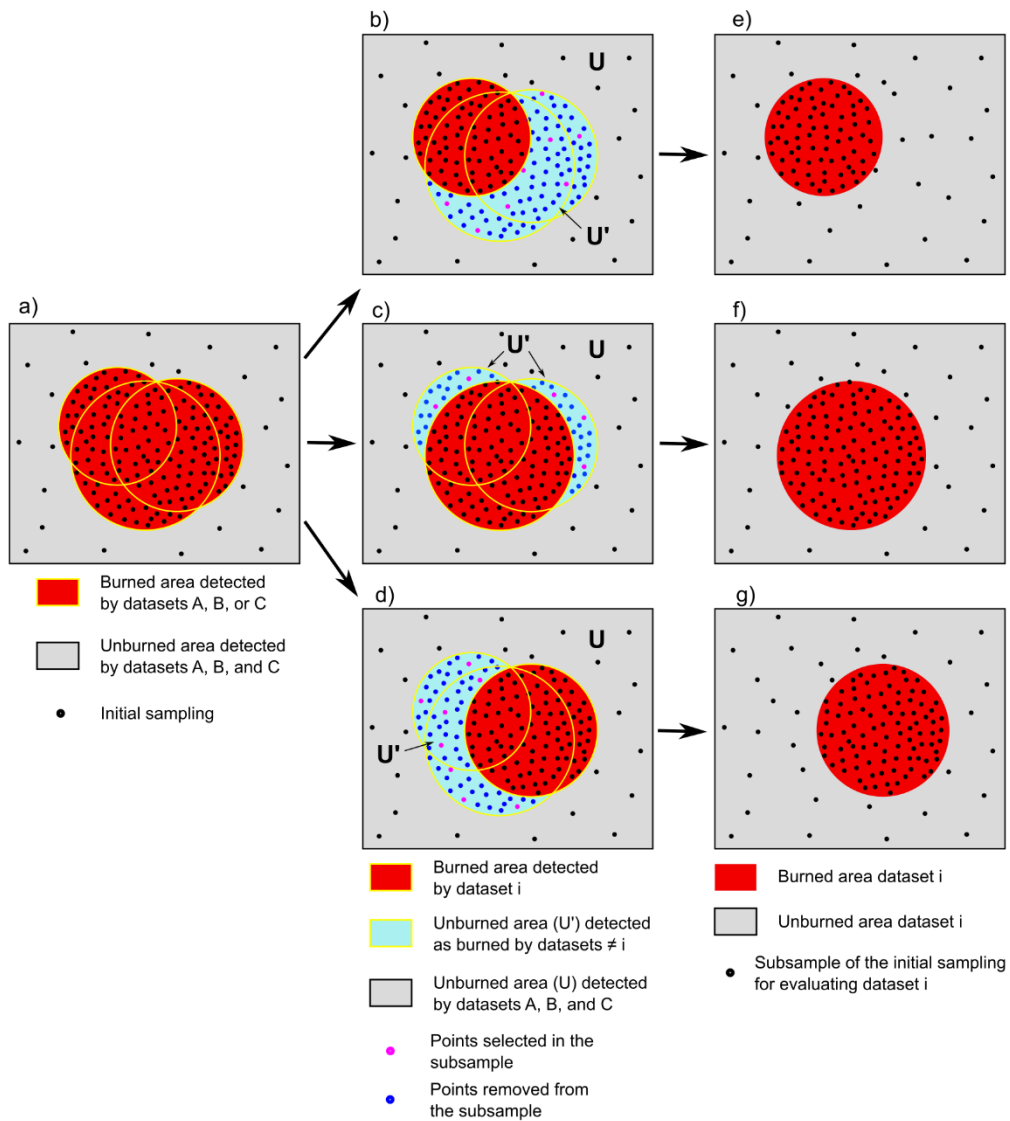
715



716

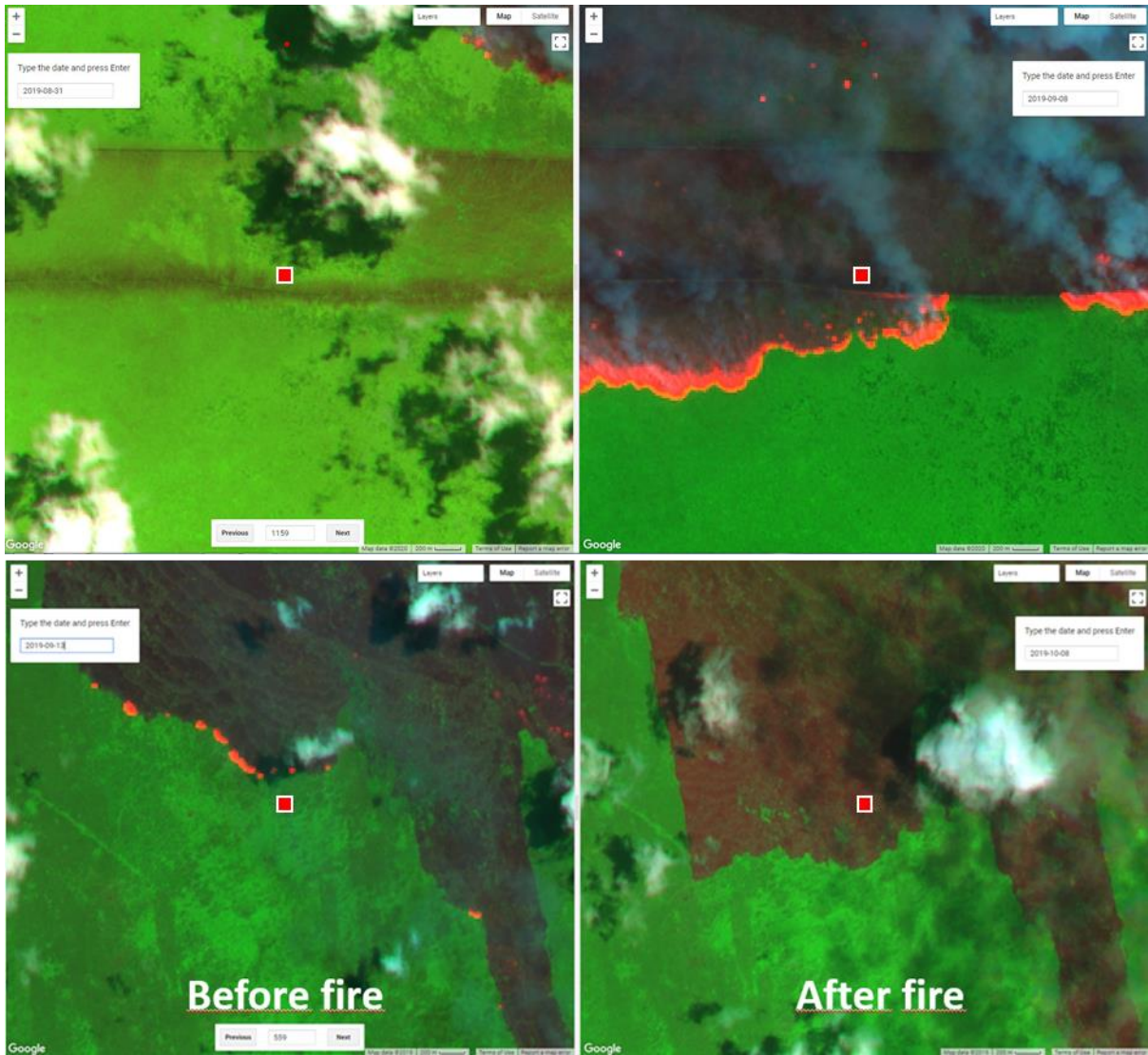
717 **Figure 2.** A schematic of Sentinel-2 time-series imagery, associated NBR values (open circles) and NBR differences between
 718 average NBR values observed before and after the central day of a 2-day moving window (blue dots). A burned pixel (20 m x
 719 20 m) is represented by a red rectangle at left. Before fire, the vegetated pixel registers positive NBR values (open circles).
 720 The NBR rapidly drops during the fire and, for a few weeks, the satellite observations show a negative NBR. The day of the
 721 year when the NBR difference observed via the moving window reaches a maximum corresponds to the moment NBR dropped
 722 (red line). This day marks a decline in the pixel's vegetation, possibly reflecting a burning event. Over time, the vegetation
 723 regenerates (re-greening) and the spectral characteristic of charred vegetation fades. Regreening can happen within days in the
 724 case of savanna grasslands, or within months in the case of forest fires on peatlands.

725
 726
 727
 728



729

730 **Figure 3.** Representation of the adjusted, stratified-sampling design for the validation of three burned area datasets (A, B, and
 731 C) against reference sites (dots). Panel (a) shows the stratified random sampling of reference sites (black points) over the
 732 combined burned area. Note that the density of samples is higher in the combined burned area than the unburned area. Panels
 733 (b), (c), and (d) show, in cyan, the area U' , being classified as unburned in a given dataset i but classified as burned in at least
 734 one other datasets $\neq i$. For a given validation of A, B, and C, the sample points in the corresponding area U' (panels (b), (c),
 735 (d)) were randomly excluded until the sampling density in the area U' equaled that of the larger unburned area U (area in gray).
 736 Panels (e), (f) and (g) show the three final, adjusted, stratified subsamples of reference points derived from the initial sample
 737 of 1298 reference points. Note that the relative areas and number of sites per class in Figure 3 do not correspond to the actual
 738 datasets being evaluated.



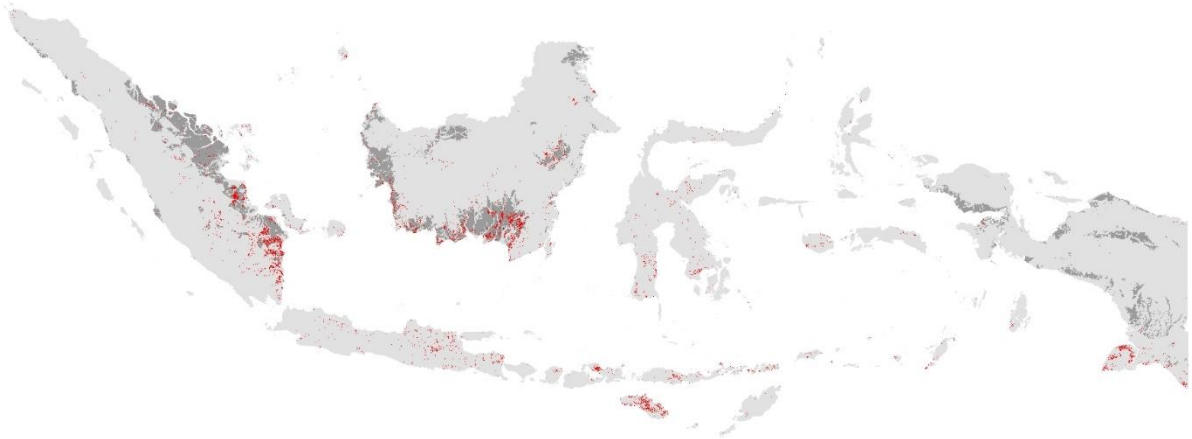
739

740 **Figure 4.** Two snapshots recording the pre-fire (left panel) and post-fire (right panel) original Sentinel-2 images acquired
 741 shortly before (13 September 2019) and shortly after (08 October 2019) fire for two reference site (red squares). Imagery
 742 displayed in RGB: SWIR, NIR, RED. Sentinel-2 provides two SWIR Bands. Band 12=2.190 μm is more suitable than Band
 743 11=1.610 μm to detect the intense heat from flaming fronts. On these image pairs, one can see flaming fronts traveling towards
 744 the reference sites (red dot) from the north on the pre fire images (left), and sharp changes in color from 'green' to 'dark red'
 745 characteristic of charred remains with continuing flaming on the post-fire images (right). Layout built using © Google Earth
 746 Engine.

747

748

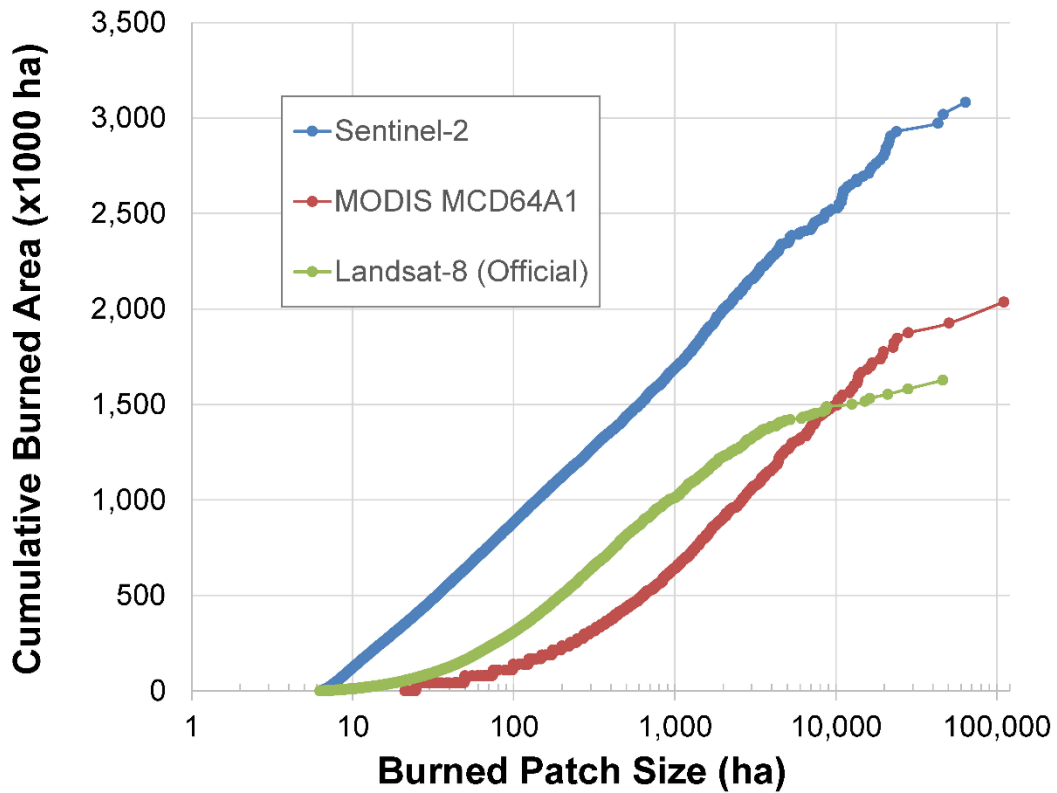
749



750

751 **Figure 5.** 2019 burned areas (red) for Indonesia (grey area) derived using a time-series of the atmospherically corrected surface
 752 reflectance multispectral images (level 2A product) taken by the Sentinel-2 A and B satellites. The spatial resolution of this
 753 map is 20 m x 20 m, and minimum mapping unit is 6.25 ha. The officially recognized peatlands extent is shown with the
 754 darkest shade of grey. A provincial breakdown of burned areas according to our map estimates and those of the Official and
 755 the MCD64A1 product are given in Figure S5.

756



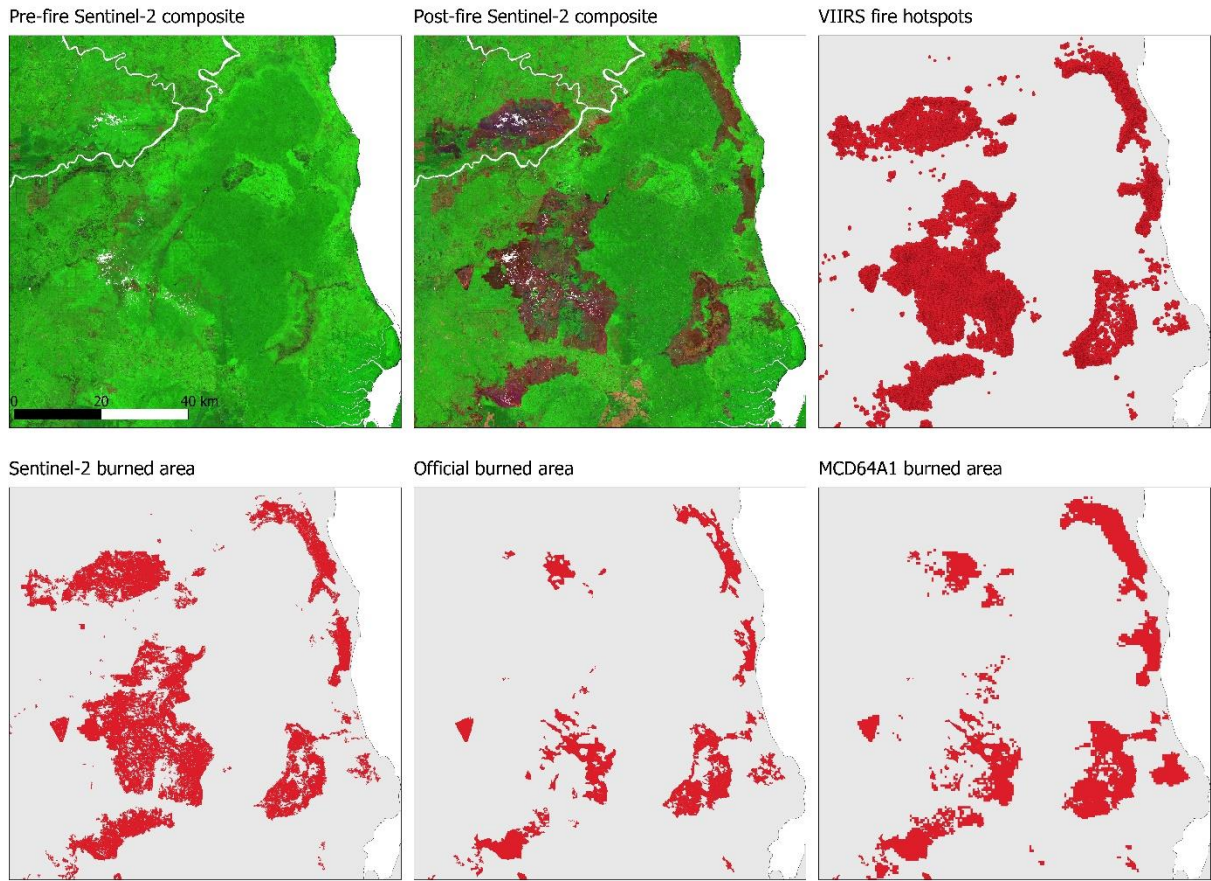
757

758 **Figure 6.** Cumulative national total burned area versus burned-scar area, for Sentinel-2, Landsat-8 (Official), and MODIS
 759 MCD64A1 burned-area estimates. Note the logarithmic axis. For a given segment of the x-axis between scar sizes X_1 and
 760 X_2 , a difference in the slopes for any two estimates is indicative of inter-estimate differences in terms of inclusivity of scars
 761 between X_1 and X_2 .

762

763

764



765

766 **Figure 7.** The pair of cloud-free pre-and post-fire Sentinel-2 composites over Berbak National Park (black line) and
 767 surrounding areas in Jambi Province (see also Inset A, Figure 1), revealing large, burned areas around Berbak National Park
 768 (areas that have transitioned from 'green' to dark 'brown/red' tones). These large burn scars have been detected by VIIRS
 769 hotspots and by the Sentinel-2 burned area map, but some have been missed by the Official and MCD64A1 datasets.
 770

771

772

773

774

775

776

777

778

779

780

781

782

783

786 **Table 1.** Adjusted, Stratified Subsamples of Reference Sites to Validate Burned-Area Estimates.

Burned-Area Estimate	Reference Sites		Total Reference Sites
	<i>In Areas Classified as Burned</i>	<i>In Areas Classified as Unburned (U & U')</i>	
Sentinel-2 (this study)	888	280	1168
MODIS MCD64A1	891	242	1133
Landsat-8 (Official)	895	182	1077

788 **Table 2.** Accuracy assessment of each of the three burned area maps performed in seven Indonesian provinces (87.60 Mha)
789 targeted for peatland restoration. The accuracy metrics were estimated with an initial total of 1,298 points randomly distributed
790 using stratified sampling. The reported metrics are: 1) the overall accuracy (OA), the user's accuracy (UA), and the producer's
791 accuracy (PA) with their 95% confidence intervals, and 2) the mapped burned area and the corrected burned area with their
792 95% confidence intervals.

	<i>SENTINEL</i>	<i>OFFICIAL</i>	<i>MCD64A1</i>
<i>OA (%)</i>	99.3 (99.1, 99.6)	98.1 (97.8, 98.5)	98.4 (98.1, 98.8)
<i>UA (%)</i>	<i>Burned</i> 97.9 (97.1, 98.8) <i>Unburned</i> 99.3 (99.1, 99.6)	<i>Burned</i> 95.1 (93.5, 96.7) <i>Unburned</i> 98.6 (98.2, 99.0)	<i>Burned</i> 76.0 (73.3, 78.7) <i>Unburned</i> 98.8 (98.5, 99.2)
<i>PA (%)</i>	<i>Burned</i> 75.6 (68.3, 83.0) <i>Unburned</i> 99.9 (99.9, 99.9)	<i>Burned</i> 49.5 (42.5, 56.6) <i>Unburned</i> 99.9 (99.9, 99.9)	<i>Burned</i> 53.1 (45.8, 60.5) <i>Unburned</i> 99.6 (99.6, 99.7)
<i>Mapped burned area (Mha)</i>	1.84	1.19	1.58
<i>Corrected burned area (Mha)</i>	2.38 (2.14, 2.61)	2.29 (1.96, 2.63)	2.27 (1.94, 2.59)
<i>Difference (Mha)</i>	0.54	1.1	0.69

794 **Table 3.** Tests statistics with respect to three-way differences in burned area scar-size frequency distributions for Sentinel,
795 MODIS, and official estimates.

Scar Size (ha)	Kruskal-Wallis H ^a
> 25	998*
> 100	335*
> 1000	14*
> 5000 ^a	0.61

797 Significance: * p<0.001

798 Notes: Scar-size thresholds in the table denote the set of scars included in a test. Tests pertain to whether frequency
799 distributions have equivalent 'distribution location', that is, position along a continuum of scar sizes. Tests thus pertain to
800 whether the estimates capture distinct realms of fire activity, assuming similarly shaped frequency distributions. Higher test
801 statistic values indicate greater probability that the estimates differ with respect to distribution location. The tree-way
802 comparisons of the estimates may flag differences where all three estimates differ or where only two of the three differ.
803 Significance is not Bonferroni corrected. (a) There are 56, 60 and 16 scars > 5000 ha for Sentinel, MCD64A1, Official
804 estimates, respectively.
805

809 **Table 4.** Test statistics with respect to two-way differences in burned area scar-size frequency distributions, with respect to
810 distribution shape and situation (Test I) or situation alone (Test II), for Sentinel estimates compared to either MCD64A1 or
811 Official estimates.

Scar Size (ha)	Sentinel vs. MCD64A1		Sentinel vs. Official			
	<i>I. Kolmogorov-Smirnov (Most Extreme Difference [positive/negative])^b</i>	<i>Z-score</i>	<i>II. Mann-Whitney U Z-score</i>	<i>I. Kolmogorov-Smirnov (Most Extreme Difference [positive/negative])^b</i>	<i>Z-score</i>	<i>II. Mann-Whitney U Z-score</i>
> 6.25	N/A			31.8** (+0.32)		-70.6**
> 25	14.7** (+0.24/-0.15)		-20.1*	13.2** (+0.18)		-28.6*
> 100	7.9** (+0.23)		-16.6*	1.6 [†] (+0.04/-0.04)		-0.57
> 1000	0.76 (+0.06/-0.03)		-0.79	1.5 [‡] (+0.01/-0.12)		-3.1*
> 5000^a	0.72 (+0.14/-0.08)		-0.77	0.70 (+0.13/-0.20)		0.10

813

814

Significance: ** p<0.0001; * p<0.001; • p<0.01; † p=0.014; ‡ p<0.05

815

Notes: Scar-size thresholds denote the cohort of scars included in a test. Test I and Test II both pertain to whether the Sentinel estimates capture distinct realms (scar-size cohorts) of fire activity compared to the other two estimates. Test I pertains to whether the scar-size frequency distribution of the Sentinel estimate has the same shape and 'distribution location' as either the MODIS or official estimate. Test II is the same but with respect to distribution location only. Distribution location refers to the situation of a frequency distribution along a continuum of scar sizes. Higher test statistics indicate greater probability that the estimates differ significantly with respect to distribution shape and/or location. Reported statistical significance is without Bonferroni corrections. a) There are 56, 60 and 16 scars > 5000 ha for Sentinel, MODIS, official estimates, respectively. (b) Largest positive and negative differences in the cumulative probability functions of Sentinel vs. MODIS or official scar-size estimates. No difference was reported where it was <0.00 absolutely.

816

817

818

819

820

821

822

823

824